Improved analyses for $\mu^- e^- \to e^- e^-$ in muonic atoms by contact interactions

Yuichi Uesaka,[1] Yoshitaka Kuno,[1] Joe Sato,[2] Toru Sato,[1,3] and Masato Yamanaka[4]
[1]*Department of Physics, Osaka University, Toyonaka, Osaka 560-0043, Japan*
[2]*Physics Department, Saitama University, 255 Shimo-Okubo, Sakura-ku, Saitama, Saitama 338-8570, Japan*
[3]*J-PARC Branch, KEK Theory Center, Institute of Particle and Nuclear Studies, KEK, Tokai, Ibaraki 319-1106, Japan*
[4]*Department of Physics, Nagoya University, Nagoya 464-8602, Japan*
(Received 4 March 2016; published 18 April 2016)

The charged lepton flavor violating (CLFV) processes of $\mu^- e^- \to e^- e^-$ decay by four Fermi contact interactions in a muonic atom for various atoms are investigated. The wave functions of bound and scattering state leptons are properly treated by solving Dirac equations with Coulomb interaction of the finite nuclear charge distributions. This new effect contributes significantly in particular for heavier atoms, where the obtained decay rate is about one order of magnitude larger than the previous estimation for ^{208}Pb. We find that, as the atomic number Z increases, the $\mu^- e^- \to e^- e^-$ decay rates increase more rapidly than the result of the previous work of Z^3, suggesting this decay as one of the promising processes to search for CLFV interaction.

DOI: 10.1103/PhysRevD.93.076006

I. INTRODUCTION

The charged lepton flavor violating (CLFV) processes are known to provide important signals on physics beyond the standard model (SM). The analysis of search for $\mu^+ \to e^+\gamma$ decays in the cosmic-ray muons by Hincks and Pontecorvo in 1947 [1] has given the first upper limit on the branching ratio of CLFV processes. Since then, the upper limits of the branching ratios of CLFV processes have been improved and now reach around the orders of $10^{-12} \sim 10^{-13}$ [2,3]. These upper limits put stringent constraints on various theoretical models beyond the SM. These CLFV searches include the processes such as $\mu^+ \to e^+\gamma$, $\mu^+ \to e^+e^-e^+$ and $\mu^- N \to e^- N$ conversion in a muonic atom. Recently, another process of $\mu^- e^- \to e^- e^-$ decay in a muonic atom has been proposed by Koike *et al.* in 2010 [4]. A unique feature of this process is that both photonic and contact leptonic interaction can be proved, and an experimentally clean signal is expected because the sum of the energies of two electrons is restricted to the muon mass minus the binding energy of the muon in a muonic atom. The measurement of this process is planned in the COMET phase-I experiment in J-PARC [5].

In Ref. [4], the decay rate of the muonic atom was evaluated by using the nonrelativistic bound state wave functions of muon and electron and the plane wave approximation of the final electrons. It was shown the decay rate increases with the atomic number Z as $\Gamma \sim Z^3$. Therefore, heavy muonic atoms would provide a great opportunity for the CLFV search. However, as is well known, the effects of the Coulomb interaction are significant for the ordinary decay of bound muons in heavy nuclei [6,7]. Since the quantitative evaluation of the decay process is needed in order to disentangle the mechanism of CLFV interaction, it is important to update the estimations of Ref. [4] by taking into account the effects of the Coulomb interactions for the relativistic leptons. The importance of the Coulomb distortion for the $\mu^- - e^-$ conversion process in a muonic atom has been reported in Refs. [8–10]. For the $\mu^- - e^-$ conversion process where the nucleus stays intact, it is sufficient to consider the s-wave muon and electron states. For $\mu^- e^- \to e^- e^-$ decay of muonic atom, on the other hand, two electrons with the energy of approximately one half of the muon mass are emitted in the final state. The angular momentum of each electron is not limited in this process. A formalism of the $\mu^- e^- \to e^- e^-$ decay with the partial wave expansion of leptons is necessary, as has been common in the nuclear beta decay and muon capture reactions [11].

In Sec. II, we summarize the relevant effective Lagrangian for the $\mu^- e^- \to e^- e^-$ process and develop a formula of the decay rate using the partial wave expansion of the lepton wave function. Our refined estimations of the $\mu^- e^- \to e^- e^-$ decay rate for the muonic atom are presented in Sec. III. Finally, our conclusion is given in Sec. IV.

II. FORMULATION

The effective Lagrangian of the CLFV process $\mu^- e^- \to e^- e^-$ is given as

$$\mathcal{L}_I = \mathcal{L}_{\text{photo}} + \mathcal{L}_{\text{contact}}, \tag{1}$$

$$\mathcal{L}_{\text{photo}} = -\frac{4G_F}{\sqrt{2}} m_\mu [A_R \bar{e_L} \sigma^{\mu\nu} \mu_R + A_L \bar{e_R} \sigma^{\mu\nu} \mu_L] F_{\mu\nu} + [\text{H.c.}], \tag{2}$$

$$\mathcal{L}_{\rm contact} = -\frac{4G_F}{\sqrt{2}}[g_1(\bar{e_L}\mu_R)(\bar{e_L}e_R) + g_2(\bar{e_R}\mu_L)(\bar{e_R}e_L) + g_3(\bar{e_R}\gamma_\mu\mu_R)(\bar{e_R}\gamma^\mu e_R) + g_4(\bar{e_L}\gamma_\mu\mu_L)(\bar{e_L}\gamma^\mu e_L) + g_5(\bar{e_R}\gamma_\mu\mu_R)(\bar{e_L}\gamma^\mu e_L) + g_6(\bar{e_L}\gamma_\mu\mu_L)(\bar{e_R}\gamma^\mu e_R)] + [\text{H.c.}], \quad (3)$$

where $G_F = 1.166 \times 10^{-5}$ GeV^{-2} is the Fermi coupling constant, and $A_{R,L}$ and g_is $(i = 1, 2, \ldots, 6)$ are dimensionless coupling constants. The left- and right-handed fields $\psi_{L/R}$ are given as $\psi_{L/R} = P_{L/R}\psi$ with $P_{L/R} = (1 \mp \gamma_5)/2$. The effective Lagrangian consists of two parts. The first part, $\mathcal{L}_{\rm photo}$, represents the photonic interaction of $\mu \to e\gamma$ types, which generates the long range $\mu - e$ interaction with one photon exchange between a muon and an electron. The second part, $\mathcal{L}_{\rm contact}$, is the four Fermi interaction. In this work, we concentrate on the contact interaction as our first attempt to examine the role of Coulomb interaction on the $\mu^- e^- \to e^- e^-$ decay of muonic atoms.

We evaluate the decay rate of two-electron emission of the muonic atom within the independent particle picture of the muonic atom and the final state. The transition amplitude is given by the matrix element of the effective CLFV interaction in Eq. (3),

$$M(\boldsymbol{p}_1, s_1, \boldsymbol{p}_2, s_2; \alpha_\mu, s_\mu, \alpha_e, s_e) \equiv \int d^3\, r \langle e^{s_1}_{\boldsymbol{p}_1} e^{s_2}_{\boldsymbol{p}_2} | \mathcal{L}_{\rm contact} | \mu^{s_\mu}_{\alpha_\mu} e^{s_e}_{\alpha_e} \rangle = -\frac{4G_F}{\sqrt{2}} \sum_{i=1}^{6} g_i \left[\int d^3 r \bar{\psi}^{e(-)}_{\boldsymbol{p}_1, s_1}(\boldsymbol{r}) O_i^A \psi^{\mu}_{\alpha_\mu, s_\mu}(\boldsymbol{r}) \bar{\psi}^{e(-)}_{\boldsymbol{p}_2, s_2}(\boldsymbol{r}) O_i^B \psi^{e}_{\alpha_e, s_e}(\boldsymbol{r}) - (1 \leftrightarrow 2) \right], \quad (4)$$

where $\psi^{e(-)}_{\boldsymbol{p},s}(\boldsymbol{r})$ is the wave function of a scattering electron with its momentum $\boldsymbol{p}$ and spin s. The superscript $(-)$ represents the incoming wave boundary condition. The wave functions of bound leptons are denoted as $\psi^l_{\alpha,s}$ with $l = \mu$, e, spin s and $\alpha = n$, κ. Here, κ represents both the orbital and the total angular momentum simultaneously [12,13]. The second term $(1 \leftrightarrow 2)$ in Eq. (4) is the exchange term obtained from the first term by exchanging the quantum numbers of final electrons. The Dirac matrix O_i^A and O_i^B for each g_i in Eq. (3) is given as

$$O_1^A = O_1^B = P_R, \quad O_2^A = O_2^B = P_L, \quad O_3^A = O_5^A = \gamma_\mu P_R, \quad O_4^A = O_6^A = \gamma_\mu P_L, \quad O_3^B = O_6^B = \gamma^\mu P_R, \quad O_4^B = O_5^B = \gamma^\mu P_L. \quad (5)$$

We assume that the muon bound state is in the $n = 1$, $\kappa = -1$ state denoted simply by $\alpha_\mu = 1S$. Since the orbit of the bound muon is about 200 times smaller than that of the electron, the $n = 1$, $\kappa = -1$ electron bound state gives the main contribution to the decay rate of the muonic atom as long as we consider the contact interaction in Eq. (3). The $\mu^- e^- \to e^- e^-$ decay rate of a muonic atom is given, with possible contributions of electron bound states of $\kappa_e = -1$ and any n included, as follows:

$$\Gamma = \frac{1}{2}\left(\sum_{s_1,s_2}\int \frac{d^3p_1 d^3p_2}{(2\pi)^3 2E_1 (2\pi)^3 2E_2}\right)\left(\frac{1}{2}\sum_{s_\mu,s_e,n}\right) \times 2\pi\delta(E_{p_1} + E_{p_2} - m_\mu - m_e + B_\mu + B_e^n) \times |M(\boldsymbol{p}_1, s_1, \boldsymbol{p}_2, s_2; 1S, s_\mu, nS, s_e)|^2, \quad (6)$$

where B_μ and B_e^n are the binding energies of the muon and electron in a muonic atom and E_{p_i} is an energy of one of the electrons with its momentum p_i. Here the initial muon spins are averaged. The normalization of the bound state wave function is given as

$$\int d^3\boldsymbol{r} \psi^l_{\alpha,s}{}^\dagger(\boldsymbol{r}) \psi^l_{\alpha,s'}(\boldsymbol{r}) = \delta_{\alpha,\alpha'}\delta_{s,s'}, \quad (7)$$

and the scattering wave function is normalized as

$$\int d^3\boldsymbol{r} \psi^{e(-)\dagger}_{\boldsymbol{p},s}(\boldsymbol{r}) \psi^{e(-)}_{\boldsymbol{p}',s'}(\boldsymbol{r}) = 2E_p(2\pi)^3\delta^3(\boldsymbol{p} - \boldsymbol{p}')\delta_{s,s'}. \quad (8)$$

The double differential decay rate with respect to the electron energy and the angle θ between emitted electrons is given as

$$\frac{d^2\Gamma_n}{dE_{p_1} d\cos\theta} = \frac{4\pi \cdot 2\pi}{8(2\pi)^5}|\boldsymbol{p}_1||\boldsymbol{p}_2| \times \sum_{s_1,s_2,s_\mu,s_e} |M(\boldsymbol{p}_1, s_1, \boldsymbol{p}_2, s_2; 1S, s_\mu, nS, s_e)|^2, \quad (9)$$

where $E_{p_2} = -E_{p_1} + m_\mu + m_e - B_\mu - B_e^n$ and is related to the total decay rate as

$$\Gamma = \frac{1}{2}\sum_n \int_{m_e}^{E^n_{\rm max}} dE_{p_1} \int_{-1}^{1} d\,\cos\theta \frac{d^2\Gamma_n}{dE_{p_1} d\cos\theta}, \quad (10)$$

where $E^n_{\rm max} = m_\mu - B_\mu - B_e^n$. The transition matrix element M is evaluated by using the partial wave expansion of the electron scattering state. The electron scattering state with the incoming boundary condition is expressed as

$$\psi^{e(-)}_{\boldsymbol{p},s}(\boldsymbol{r}) = \sum_{\kappa,\nu,m} 4\pi i^{l_\kappa}(l_\kappa, m, 1/2, s|j_\kappa,\nu) Y^*_{l_\kappa,m}(\hat{p}) e^{-i\delta_\kappa}\psi^\kappa_{p,\nu}(\boldsymbol{r}), \tag{11}$$

where δ_κ is a phase shift for partial wave κ. $(l_\kappa, m, 1/2, s|j_\kappa,\nu)$ and $Y_{l_\kappa,m}(\hat{p})$ are Clebsch-Gordan coefficients and spherical harmonics, respectively. Furthermore, the wave function $\psi^\kappa_{p,\nu}(\boldsymbol{r})$, where the subscripts p, ν mean a momentum of the electron and a spin of the partial wave, is written with the radial part $g^\kappa_p(r)$, $f^\kappa_p(r)$ and the angular-spin part χ_κ [12,13] as follows:

$$\psi^\kappa_{p,\nu}(\boldsymbol{r}) = \begin{pmatrix} g^\kappa_p(r)\chi^\nu_\kappa(\hat{r}) \\ i f^\kappa_p(r)\chi^\nu_{-\kappa}(\hat{r}) \end{pmatrix}. \tag{12}$$

Similarly, the bound state wave function is given as

$$\psi^l_{\alpha,s}(\boldsymbol{r}) = \begin{pmatrix} g^\kappa_{n,l}(r)\chi^s_\kappa(\hat{r}) \\ i f^\kappa_{n,l}(r)\chi^s_{-\kappa}(\hat{r}) \end{pmatrix}, \tag{13}$$

where the subscript l is for muon $l=\mu$ or electron $l=e$ and s is a spin of the lepton. The radial wave functions $g^\kappa(r)$ and $f^\kappa(r)$ are obtained by solving the following Dirac equation with the Coulomb potential $V_C(r)$ for the appropriate boundary condition:

$$\frac{dg^\kappa(r)}{dr} + \frac{1+\kappa}{r} g^\kappa(r) - (E + m + eV_C(r)) f^\kappa(r) = 0, \tag{14}$$

$$\frac{df^\kappa(r)}{dr} + \frac{1-\kappa}{r} f^\kappa(r) - (E - m + eV_C(r)) g^\kappa(r) = 0. \tag{15}$$

Using the partial wave expansion of the scattering wave function the transition amplitude can be written as follows:

$$\begin{aligned} M(\boldsymbol{p}_1, s_1, \boldsymbol{p}_2, s_2; 1S, s_\mu, nS, s_e) = {} & 2\sqrt{2}G_F \sum_{\kappa_1,\kappa_2,\nu_1,\nu_2,m_1,m_2} (4\pi)^2 (-i)^{l_{\kappa_1}+l_{\kappa_2}} e^{i(\delta_{\kappa_1}+\delta_{\kappa_2})} \\ & \times Y_{l_{\kappa_1},m_1}(\hat{p}_1) Y_{l_{\kappa_2},m_2}(\hat{p}_2) (l_{\kappa_1}, m_1, 1/2, s_1|j_{\kappa_1},\nu_1)(l_{\kappa_2}, m_2, 1/2, s_2|j_{\kappa_2},\nu_2) \\ & \times \sum_{J,M} (j_{\kappa_1},\nu_1, j_{\kappa_2},\nu_2|J,M)(j_{-1}, s_\mu, j_{-1}, s_e|J,M) \\ & \times \frac{2\sqrt{(2j_{\kappa_1}+1)(2j_{\kappa_2}+1)}}{4\pi} \sum_{i=1}^{6} g_i W_i(J,\kappa_1,\kappa_2, E_{p_1}). \end{aligned} \tag{16}$$

Here $W_i(J,\kappa_1,\kappa_2,E_{p_1})$ is the transition matrix element for the g_i term that includes both direct and exchange terms. We introduce the function $Z_{ABCD}(L,S,J)$, which consists of the radial overlap integral, 9j and parity Clebsch-Gordan coefficients as

$$\begin{aligned} Z_{ABCD}(L,S,J) = {} & \int_0^\infty dr\, r^2 A^{\kappa_1}_{p_1}(r) B^{-1}_{1,\mu}(r) C^{\kappa_2}_{p_2}(r) D^{-1}_{n,e}(r) \\ & \times \sqrt{(2l^A_{\kappa_1}+1)(2l^B_{-1}+1)(2l^C_{\kappa_2}+1)(2l^D_{-1}+1)} \\ & \times (l^A_{\kappa_1}, 0, l^C_{\kappa_2}, 0|L,0)(l^B_{-1}, 0, l^D_{-1}, 0|L,0) \\ & \times \begin{Bmatrix} l^A_{\kappa_1} & 1/2 & j_{\kappa_1} \\ l^C_{\kappa_2} & 1/2 & j_{\kappa_2} \\ L & S & J \end{Bmatrix} \begin{Bmatrix} l^B_{-1} & 1/2 & 1/2 \\ l^D_{-1} & 1/2 & 1/2 \\ L & S & J \end{Bmatrix}. \end{aligned} \tag{17}$$

Here A and C represent the electron scattering states with momentum p_1 and p_2 and B and D represent the bound states of the muon and electron. The radial wave functions $A(r)$, $B(r)$, $C(r)$, and $D(r)$ are either $g(r)$ or $f(r)$ introduced in Eqs. (12)–(13). The angular momentum l^h_κ is defined as

$$l^h_\kappa = \begin{cases} l_{+\kappa} & \text{for } h = g, \\ l_{-\kappa} & \text{for } h = f. \end{cases} \tag{18}$$

The amplitude W_i for $i = 1,\ldots,6$ is written by using linear combination of Z as

$$W_1(J) = \frac{1}{2}\{X^-_\alpha(J,0,J) - X^+_\beta(J,0,J) + i[Y^+_\alpha(J,0,J) + Y^+_\beta(J,0,J)]\}, \tag{19}$$

$$W_2(J) = \frac{1}{2}\{X^-_\alpha(J,0,J) - X^+_\beta(J,0,J) - i[Y^+_\alpha(J,0,J) + Y^+_\beta(J,0,J)]\}, \tag{20}$$

$$W_3(J) = 2\{X^-_\alpha(J,0,J) + X^+_\beta(J,0,J) - i[Y^+_\alpha(J,0,J) - Y^+_\beta(J,0,J)]\}, \tag{21}$$

$$W_4(J) = 2\{X^-_\alpha(J,0,J) + X^+_\beta(J,0,J) + i[Y^+_\alpha(J,0,J) - Y^+_\beta(J,0,J)]\}, \tag{22}$$

$$W_5(J) = 3\sum_{L=|J-1|}^{J+1} X_\beta^-(L,1,J) - X_\alpha^+(J,0,J) + i\left[3\sum_{L=|J-1|}^{J+1} Y_\alpha^-(L,1,J) + Y_\beta^-(J,0,J)\right], \tag{23}$$

$$W_6(J) = 3\sum_{L=|J-1|}^{J+1} X_\beta^-(L,1,J) - X_\alpha^+(J,0,J) - i\left[3\sum_{L=|J-1|}^{J+1} Y_\alpha^-(L,1,J) + Y_\beta^-(J,0,J)\right], \tag{24}$$

with

$$X_\alpha^\pm(L,S,J) = Z_{gggg}(L,S,J) + Z_{ffff}(L,S,J) \pm [Z_{gfgf}(L,S,J) + Z_{fgfg}(L,S,J)], \tag{25}$$

$$X_\beta^\pm(L,S,J) = Z_{ggff}(L,S,J) + Z_{ffgg}(L,S,J) \pm [Z_{gffg}(L,S,J) + Z_{fggf}(L,S,J)], \tag{26}$$

$$Y_\alpha^\pm(L,S,J) = Z_{ggfg}(L,S,J) - Z_{ffgf}(L,S,J) \pm [Z_{fggg}(L,S,J) - Z_{gfff}(L,S,J)], \tag{27}$$

$$Y_\beta^\pm(L,S,J) = Z_{gggf}(L,S,J) - Z_{fffg}(L,S,J) \pm [Z_{gfgg}(L,S,J) - Z_{fgff}(L,S,J)]. \tag{28}$$

Since we assume the bound states of the muon and electron are both in the $\kappa = -1$ state, the total angular momentum J can be $J = 0$ or 1 and $X^\pm_{\alpha(\beta)}$ and $Y^\pm_{\alpha(\beta)}$ are nonzero only for even L and odd L respectively. It is noticed that only the $S = 0$ term contributes for W_1, W_2, W_3, and W_4, while both $S = 0$ and 1 terms contribute for W_5 and W_6.

After summing the spins of leptons, we yield the differential transition rate,

$$\begin{aligned}\frac{d^2\Gamma_n}{dE_{p_1} d\cos\theta} = \frac{G_F^2}{\pi^3}|\boldsymbol{p}_1||\boldsymbol{p}_2| \sum_{\kappa_1,\kappa_2,\kappa_1',\kappa_2',J,l} &(2J+1)(2j_{\kappa_1}+1)(2j_{\kappa_2}+1)(2j_{\kappa_1'}+1)(2j_{\kappa_2'}+1) \\ &\times \frac{1+(-1)^{l_{\kappa_1}+l_{\kappa_1'}+l}}{2}\frac{1+(-1)^{l_{\kappa_2}+l_{\kappa_2'}+l}}{2} i^{-l_{\kappa_1}-l_{\kappa_2}+l_{\kappa_1'}+l_{\kappa_2'}} e^{i(\delta_{\kappa_1}+\delta_{\kappa_2}+\delta_{\kappa_1'}+\delta_{\kappa_2'})} \\ &\times (j_{\kappa_1}, 1/2, j_{\kappa_1'}, -1/2|l,0)(j_{\kappa_2}, 1/2, j_{\kappa_2'}, -1/2|l,0) W(j_{\kappa_1} j_{\kappa_2} j_{\kappa_1'} j_{\kappa_2'}; Jl) \\ &\times (-1)^{J-j_{\kappa_2}-j_{\kappa_2'}} \sum_{i=1}^{6} g_i W_i(J,\kappa_1,\kappa_2,E_{p_1},n) \sum_{i'=1}^{6} g_{i'}^* W_{i'}^*(J,\kappa_1',\kappa_2',E_{p_1},n) P_l(\cos\theta),\end{aligned} \tag{29}$$

where $P_l(x)$ is Legendre polynomial and W is Racah coefficient, and we can estimate the angular integral analytically and obtain the following formula for the decay rate of $\mu^- e^- \to e^- e^-$ of a muonic atom,

$$\Gamma = \frac{G_F^2}{\pi^3}\sum_n \int_{m_e}^{E^n_{\max}} dE_{p_1}|\boldsymbol{p}_1||\boldsymbol{p}_2| \sum_{J,\kappa_1,\kappa_2} (2J+1)(2j_{\kappa_1}+1)(2j_{\kappa_2}+1)\left|\sum_{i=1}^{6} g_i W_i(J,\kappa_1,\kappa_2,E_{p_1},n)\right|^2. \tag{30}$$

III. NUMERICAL RESULTS

At first, we study the transition density $\rho_{\rm tr}(r)$ given by the product of lepton wave functions as

$$\rho_{\rm tr}(r) = g_{p_1}^{-1}(r) g_\mu^{-1}(r) g_{p_2}^{-1}(r) g_e^{-1}(r) \tag{31}$$

to find the role of the Coulomb interaction on the lepton wave function. Here we take the most important transition matrix element of the $1S$ electron and muon to the $\kappa = -1$ electrons ($\mu^-(1S) + e^-(1S) \to e^-(\kappa = -1) + e^-(\kappa = -1)$), where the two electrons are equally sharing the energy $E_{p_1} = E_{p_2} = (m_\mu + m_e - B_\mu^{1S} - B_e^{1S})/2$. We examine four models for the lepton wave functions shown in Table I. In model I, the bound state wave functions of the muon and electron are calculated in the nonrelativistic approximation (Non. Rel.) with Coulomb interaction of point nuclear charge (Point Coul.) and the electron scattering states are in the plane wave approximation (PLW). Then the wave function of the scattering state is replaced by the solution of the Dirac equation (Rel.) in model II. In model III, both the bound state and the scattering state lepton wave

TABLE I. Models for the lepton wave functions.

Model	Bound state	Scattering state
I	Non. Rel./Point Coul.	Rel./PLW
II	Non. Rel./Point Coul.	Rel./Point Coul.
III	Rel./Point Coul.	Rel./Point Coul.
IV	Rel./Uniform Coul.	Rel./Uniform Coul.

functions are calculated from the Dirac equation with point nuclear charge. Finally, we used the uniform nuclear charge distribution (Uniform Coul.) in model IV.

The transition densities of the four models for the $\mu^- e^- \to e^- e^-$ decay of the ^{208}Pb muonic atom are shown in Fig. 1. The dashed curve shows transition density in model I that simulates the previous analysis. By including the Coulomb attraction for scattering electrons in model II, the transition density is enhanced around the muon Bohr radius as shown by the dash-dotted curve. Further we use the consistent lepton wave functions of the Dirac equation with point nuclear charge in model III. The transition density becomes very large as shown by the dash-two-dotted curve, which is $1/3$ of the actual transition density. However, the use of point nuclear charge would not be appropriate for an atom of large Z, where the Bohr radius of the muon can be comparable to the nuclear radius. The solid curve shows our final result by using a finite charge distribution of nucleus in model IV. The peak position of the transition density is shifted toward larger r compared with that of point nuclear charge. Here the charge distribution of nucleus is taken as a uniform distribution as

$$\rho_C(r) = \frac{3Ze}{4\pi R^3}\theta(R-r). \tag{32}$$

We use $R = 1.2A^{1/3}$ for mass number A. For each Z, we take the mass number A of the most abundant isotope [14], e.g., $A = 208$ for $Z = 82$.

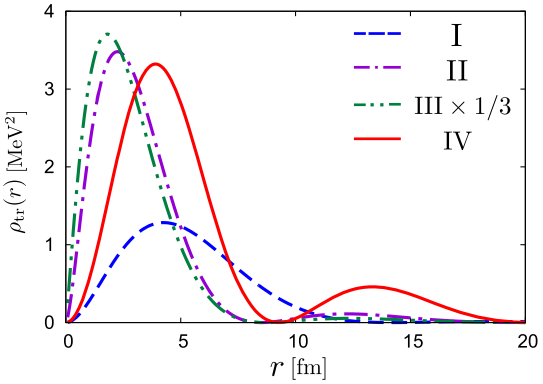

FIG. 1. The transition density $\rho(r)r^2$ for the $\mu^-(1S) + e^-(1S) \to e^-(\kappa = -1) + e^-(\kappa = -1)$. The dashed, dash-dotted, dash-two-dotted, and solid curves show the transition density in models I–IV, respectively.

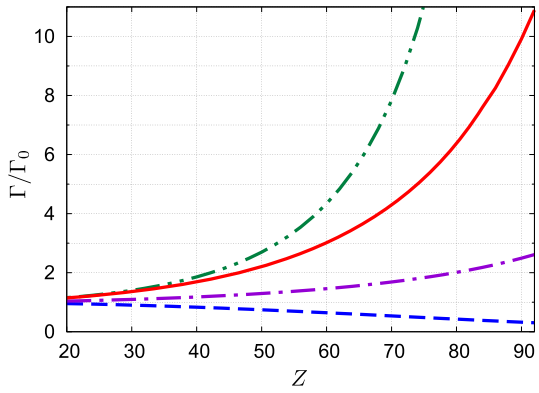

FIG. 2. The atomic number (Z) dependence of the ratio of the decay rate Γ/Γ_0. The dashed, dash-dotted, dash-two-dotted, and solid curves show the transition density in models I–IV, respectively. We note that the factor $1/3$ has not been multiplied to the dash-two-dotted curve.

An analytic formula of the $\mu^- e^- \to e^- e^-$ decay rate of the muonic atom is given in the previous work [4] as

$$\Gamma_0 = \frac{m_\mu}{8\pi^2}(Z-1)^3\alpha^3(G_F m_\mu^2)^2\left(\frac{m_e}{m_\mu}\right)^3 G, \tag{33}$$

where $G \equiv G_{12} + 16G_{34} + 4G_{56} + 8G'_{14} + 8G'_{23} - 8G'_{56}$ with $G_{ij} \equiv |g_i|^2 + |g_j|^2$ and $G'_{ij} \equiv \mathrm{Re}(g_i^* g_j)$. The formula shows that the decay rate is proportional to $(Z-1)^3$. The formula was obtained by using the nonrelativistic bound state of the muon and $1S$ electron with a point nuclear charge and the plane wave approximation for the final electrons.

The decay rate Γ obtained in this work is shown in Fig. 2. Here the ratios Γ/Γ_0 are plotted. We retain only the term of g_1 and set the other gs to zero. The contribution of the dominant $1S$ bound electron is included. The dashed curve in Fig. 2 shows the decay rate evaluated with model I. The ratio for model I deviates from unity for large Z because of using the finite size bound muon wave function instead of using the plane wave in the previous estimation. When we replace the plane wave electrons with the Dirac wave function for point nuclear charge (II), the decay rate increases as shown in the dash-dotted curve. When both bound and scattering states are described by the Dirac equation that includes the Coulomb interaction of point nuclear charge (III), the decay rate is even more enhanced as shown in the dash-two-dotted curve. A realistic description of Γ/Γ_0 is obtained by using the uniform nuclear charge distribution in model IV as shown in the solid curve in Fig. 2.

The results show that, while Γ_0 gives reasonable estimation for smaller $Z \sim 20$, the Z dependence of the Γ is stronger than $(Z-1)^3$. The ratio Γ/Γ_0 is about 7.0 for the ^{208}Pb. We found slightly different Z dependence of Γ for two types of the effective CLFV contact interaction. The

TABLE II. The convergence property of the partial wave expansion of Γ/Γ_0.

Nuclei	$\lvert\kappa\rvert \le 1$	$\lvert\kappa\rvert \le 5$	$\lvert\kappa\rvert \le 10$	$\lvert\kappa\rvert \le 20$
^{40}Ca	0.141	0.847	1.11	1.15
^{120}Sn	0.731	2.17	2.21	2.21
^{208}Pb	2.89	6.94	6.96	6.96

interaction of the g_i term with $i = 1, 2, 3, 4$, which leads to the same helicity states of two electrons, gives $\Gamma/\Gamma_0 \sim 7.0(1.1)$ for ^{208}Pb (^{40}Ca). For the g_i term with $i = 5, 6$, where the opposite helicity states of electrons are emitted, the decay rate is $\Gamma/\Gamma_0 \sim 6.3(1.1)$ for ^{208}Pb (^{40}Ca). Therefore, Z dependence of the decay rate for $g_1 \sim g_4$ is slightly stronger than that of g_5 and g_6.

All the results of the decay rate were obtained by including a sufficiently large number of partial waves of final electrons. The convergence properties of the decay rate against the number of partial waves included are shown in Table II. The number of partial waves needed to obtain convergent results was $|\kappa| \sim 6$ for Pb and Sn and $|\kappa| \sim 13$ for Ca. This happens because the muon Bohr radius is increasing for decreasing Z.

We have also examined the realistic form of the distribution of nuclear charge using the Woods-Saxon form,

$$\rho_C(r) = \rho_0 \left[1 + \exp\left(\frac{r-c}{z}\right)\right]^{-1}, \tag{34}$$

for ^{40}Ca, ^{120}Sn, and ^{208}Pb. The parameters, c and z, and the ratio of the decay rate Γ/Γ_0 are listed in Table III. The modification of the decay rate using Woods-Saxon form charge distribution in place of uniform distribution is less than 1%.

The results shown so far were obtained including only the main transitions where the initial electrons are bound in the $1S$ state. The contributions of the electrons from the higher shell $2S, 3S\ldots$ are estimated within the independent particle model for the atomic electrons. Contributions of higher shell electrons increase the transition rate by ~20% as shown in Table III, which is consistent with the result of the previous work.

TABLE III. The parameters of the charge distribution of the Woods-Saxon form and the ratio of the decay rates Γ/Γ_0 for ^{40}Ca, ^{120}Sn, and ^{208}Pb [15]. In the fourth (fifth) column, the Γ/Γ_0 including the contribution of the $1S$ ($1S$ and higher shells) is shown.

Nuclei	c [fm]	z [fm]	Γ/Γ_0 (only $1S$)	$1S + 2S + \cdots$
^{40}Ca	3.51(7)	0.563	1.15	1.35
^{120}Sn	5.315(25)	0.576(11)	2.21	2.67
^{208}Pb	6.624(35)	0.549(8)	6.96	8.78

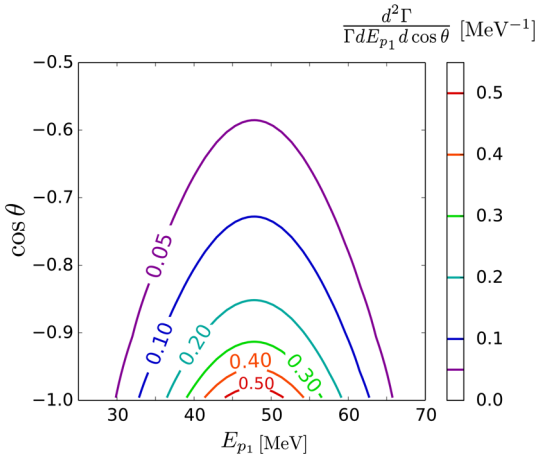

FIG. 3. The energy and angular distribution of emitted electrons for the ^{208}Pb by using g_1 type interaction.

The energy and angular distribution of the electron calculated from the double differential decay rate in Eq. (9) for the ^{208}Pb is shown in Fig. 3. The two final electrons are mainly emitted with the same energy in an opposite direction, since the momentum carried by the bound two leptons is minimized in this configuration. The electron energy spectrum normalized by decay rate $d\Gamma/dE/\Gamma$ and the angular distribution between the two electrons are shown in Figs. 4–5 for models IV (solid) and I (dashed). The maximum of the energy distribution is around half of the total energy $m_\mu + m_e - B_\mu^{1S} - B_e^{1S}$. Most of the final electrons are emitted in the opposite directions. The shapes of the energy distribution and the angular distribution are significantly different from models I and IV. The angular and energy distributions in model IV become narrower than those of model I. This is because the muon is less bound for finite range nuclear charge distribution, and therefore it has a smaller high momentum component.

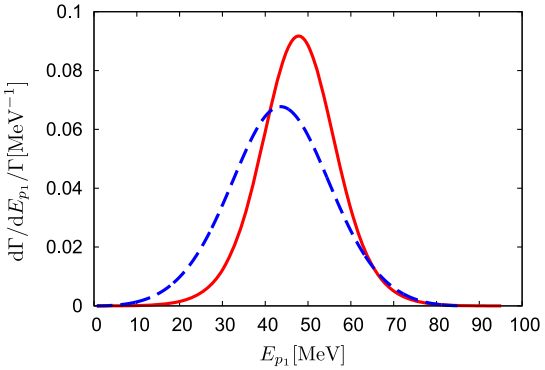

FIG. 4. The normalized energy distribution of the electron for the ^{208}Pb. The solid (red) curve and the dashed (blue) curve are obtained by using models IV and I, respectively. The g_1 term is included and all bound S state electrons are taken into account.

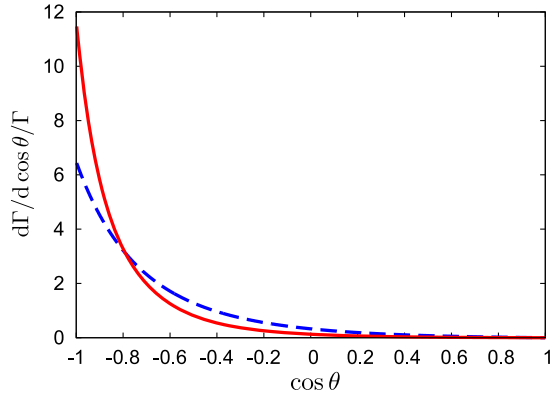

FIG. 5. The normalized angular distribution of emitted electrons for the ^{208}Pb. The other features are the same as those in Fig. 4.

For the interaction that leads to the same chirality of final electrons, i.e., $g_1 \sim g_4$ terms of Eq. (4), the Pauli principle prevents the final electron from having the same momentum. On the other hand, in g_5 and g_6 terms that lead to electrons with opposite chiralities, this does not apply. A difference between two interaction terms appears near $\cos\theta = 1$ as seen in Fig. 6.

Finally, we evaluate upper limits for the branching ratio of the $\mu^- e^- \to e^- e^-$ decay of a muonic atom. The branching ratio of $\mu^- e^- \to e^- e^-$ is defined by using the $\mu^- e^- \to e^- e^-$ decay rate of muonic atom $\Gamma(\mu^- e^- \to e^- e^-)$ [Γ given in Eq. (6)] and the total decay rate of muonic atom $1/\tilde{\tau}_\mu$,

$$Br(\mu^- e^- \to e^- e^-) \equiv \tilde{\tau}_\mu \Gamma(\mu^- e^- \to e^- e^-). \quad (35)$$

We estimate the strength of the CLFV interaction from the current upper limit of the branching ratio of $\mu^+ \to e^+ e^+ e^-$. The branching ratio $Br(\mu^+ \to e^+ e^+ e^-)$ is given as

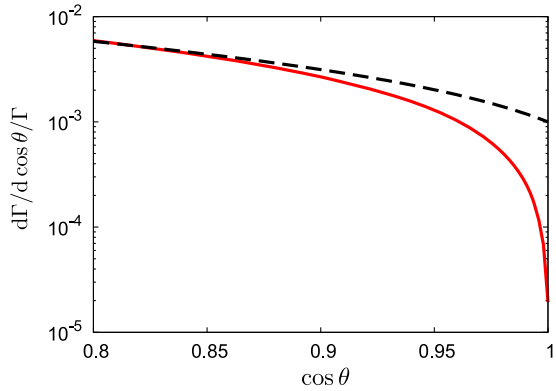

FIG. 6. The angular distribution of emitted electrons for the ^{208}Pb. The angular distribution due to the (g_1-g_4) terms is shown in the solid (red) curve, and that of the (g_5-g_6) terms is shown in the dashed (black) curve.

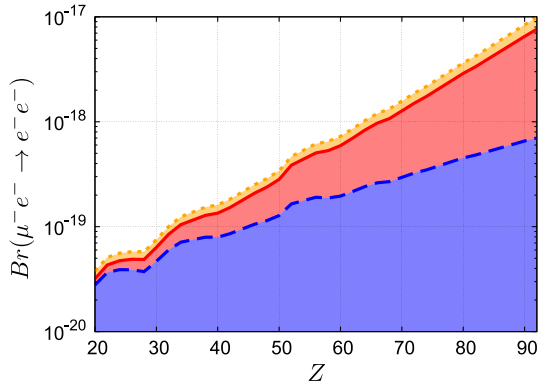

FIG. 7. Upper limits of $Br(\mu^- e^- \to e^- e^-)$. The dashed (blue) curve shows the result of previous work [4]. Our results including only $1S$ electrons and all $1S$ electrons are shown by the solid (red) curve and the dotted (orange) curve, respectively.

$$Br(\mu^+ \to e^+ e^+ e^-) \equiv \tau_\mu \Gamma(\mu^+ \to e^+ e^+ e^-). \quad (36)$$

Here $\Gamma(\mu^+ \to e^+ e^+ e^-)$ and $1/\tau_\mu$ are the decay rate of $\mu^+ \to e^+ e^+ e^-$ and total decay rate of the free muon, respectively. Using the contact CLFV interaction in Eq. (3), the branching ratio $Br(\mu^+ \to e^+ e^+ e^-)$ is given as [16]

$$Br(\mu^+ \to e^+ e^+ e^-) = \frac{1}{8}(G_{12} + 16G_{34} + 8G_{56}). \quad (37)$$

Keeping only the g_1 term of the CLFV interaction, we can express the branching ratio of $\mu^- e^- \to e^- e^-$ decay of the muonic atom as [4]

$$Br(\mu^- e^- \to e^- e^-) \simeq 192\pi(Z-1)^3\alpha^3 \left(\frac{m_e}{m_\mu}\right)^3 \frac{\tilde{\tau}_\mu}{\tau_\mu}\frac{\Gamma}{\Gamma_0} \times Br(\mu^+ \to e^+ e^+ e^-). \quad (38)$$

Here we used $\tau_\mu = 192\pi^3/(G_F^2 m_\mu^5) = 2.197 \times 10^{-6}$ [s]. The upper limit of $Br(\mu^- e^- \to e^- e^-)$ can be estimated by using the current upper limit of the branching ratio $Br(\mu^+ \to e^+ e^+ e^-)$.

The upper limits of the branching ratio of the previous work (dashed curve) and our results with $1S$ (solid curve) and all nS electrons (dotted curve) are shown in Fig. 7. Here we used the result of the SINDRUM experiment $Br(\mu^+ \to e^+ e^+ e^-) < 1.0 \times 10^{-12}$ [17] and the data of the lifetime of muonic atoms $\tilde{\tau}_\mu$ given in [18]. For ^{208}Pb (^{238}U), the branching ratios $Br(\mu^- e^- \to e^- e^-)$ considering only $1S$ electrons and all electrons are 3.3×10^{-18} (6.9×10^{-18}) and 4.2×10^{-18} (9.8×10^{-18}), respectively. $Br(\mu^- e^- \to e^- e^-)$ reaches about 10^{-17} for ^{238}U.

IV. CONCLUSION

We have made an improved study on the $\mu^- e^- \to e^- e^-$ decay in muonic atoms. Coulomb interaction of leptons with finite nuclear charge distributions is taken into account by using the standard multipole expansion formalism and the numerical solutions of Dirac equations for both the electron and muon wave functions. The effects of Coulomb distortion of the emitted electron and relativistic treatments of the bound leptons are significantly important for quantitative estimations of the decay rate. Enhancements of the decay rates of about nine and 14 times for ^{208}Pb and ^{238}U respectively compared with the previous analysis are obtained due to the enhanced overlap integrals of the lepton wave functions. We also found that different helicity structures of the CLFV interaction generate sizable difference in the Z-dependence of the decay rate and also the angular distribution of the emitted electrons. Finally, the upper limits of the branching ratio of the $\mu^- e^- \to e^- e^-$ decay of the muonic atom were estimated.

In this work we have included only the four Fermi CLFV interaction. It is important to estimate the photonic interaction that generates long range interactions between the bound muon and many electrons in an atom. In addition to the decay rates, it would be of great interest to find some other observables that may be useful to discriminate photonic and contact interactions and also various terms of the effective CLFV interactions. These issues are in progress and will be discussed in a separate paper.

ACKNOWLEDGMENTS

This work was supported by the MEXT KAKENHI Grant No. 25105009 (J. S.) and No. 25105010 (T. S.), and the JSPS KAKENHI Grant No. 24340044 (J. S.), No. 25000004 (Y. K.), and No. 25003345 (M. Y.). T. S. and Y. U. thank Dr. S. Nakamura for valuable comments.

[1] E. P. Hincks and B. Pontecorvo, Phys. Rev. **73**, 257 (1948).
[2] Y. Kuno and Y. Okada, Rev. Mod. Phys. **73**, 151 (2001).
[3] Y. Kuno, Prog. Theor. Exp. Phys. **2013**, 022C01 (2013).
[4] M. Koike, Y. Kuno, J. Sato, and M. Yamanaka, Phys. Rev. Lett. **105**, 121601 (2010).
[5] R. Abramishili *et al.*, COMET phase-I technical design report, Report No. 2015-1, 2015.
[6] R. W. Huff, Ann. Phys. (N. Y.) **16**, 288 (1961).
[7] R. Watanabe, M. Fukui, H. Ohtsubo, and M. Morita, Prog. Theor. Phys. **78**, 114 (1987).
[8] R. Kitano, M. Koike, and Y. Okada, Phys. Rev. D **66**, 096002 (2002).
[9] O. Shanker, Phys. Rev. D **20**, 1608 (1979).
[10] A. Czarnecki, W. J. Marciano, and K. Melnikov, AIP Conf. Proc. **435**, 409 (1998).
[11] K. Koshigiri, N. Nishimura, H. Ohtsubo, and M. Morita, Nucl. Phys. **A319**, 301 (1979).
[12] M. E. Rose, *Relativistic Electron Theory* (John Wiley & Sons, New York, 1961).
[13] M. E. Rose, *Elementary Theory of Angular Momentum* (John Wiley & Sons, New York, 1957).
[14] M. Berglund and M. E. Wieser, Pure Appl. Chem. **83**, 397 (2011).
[15] C. W. De Jager, H. De Vries, and C. De Vries, At. Data Nucl. Data Tables **14**, 479 (1974).
[16] Y. Okada, K. I. Okumura, and Y. Shimizu, Phys. Rev. D **61**, 094001 (2000).
[17] U. Bellgardt *et al.*, Nucl. Phys. **B299**, 1 (1988).
[18] T. Suzuki, D. F. Measday, and J. P. Roalsvig, Phys. Rev. C **35**, 2212 (1987).